A Neuropilin-1 Antagonist Exerts Antitumor Immunity by Inhibiting the Suppressive Function of Intratumoral Regulatory T Cells

Keunok Jung[1], Jeong-Ah Kim[2], Ye-Jin Kim[2], Hyun Woo Lee[3], Chul-Ho Kim[2,4], Seokjin Haam[5], and Yong-Sung Kim[1,2]

ABSTRACT

Regulatory T cells (Treg) are targeted for cancer immunotherapy because they suppress antitumor immunity. Although the importance of neuropilin-1 (NRP1) in the stability and function of intratumoral Tregs is well-documented, targeting of NRP1$^+$ Tregs for anticancer immunotherapy has not been well explored. Here, we found that an NRP1 antagonist [Fc(AAG)-TPP11], generated by fusion of the NRP1-specific binding peptide TPP11 with the C-terminus of an effector function–deficient immunoglobulin Fc(AAG) variant, inhibits intratumoral NRP1$^+$ Treg function and stability. Fc(AAG)-TPP11 triggered the internalization of NRP1, reducing its surface expression on Tregs and thereby inhibiting the suppressive function of Tregs. In two murine syngeneic tumor models, Fc(AAG)-TPP11 retarded tumor growth, comparable with a Treg-depleting anti–CTLA-4 antibody, without noticeable toxicity. Fc(AAG)-TPP11 inhibited NRP1-dependent Treg function, inducing unstable intratumoral Tregs, with reduced expression of Foxp3 and enhanced production of IFNγ, which subsequently increased the functionality and frequency of intratumoral CD8$^+$ T cells. We also observed selective expression of NRP1 on Tregs isolated from human tumors, but not from the blood of healthy donors and patients with cancer, as well as *ex vivo* inhibition of intratumoral NRP1$^+$ Treg function by Fc(AAG)-TPP11. Our results suggest that the NRP1 antagonist Fc(AAG)-TPP11 has therapeutic potential for the inhibition of intratumoral NRP1$^+$ Tregs with limited unfavorable effects on peripheral Tregs.

Introduction

CD4$^+$ CD25$^+$ regulatory T cells (Treg), characterized by the expression of the master regulatory transcription factor Foxp3, are immune suppressive and play central roles in maintaining self-tolerance and immune homeostasis (1). Tumors take advantage of the immune-suppressive function of Tregs, which inhibit anticancer immunity in the tumor microenvironment (TME; ref. 2). Tumor-infiltrated Tregs are activated in the TME and display different phenotypes from peripheral Tregs (3). Tumor-infiltrated Tregs suppress antitumor effector cells, such as CD4$^+$ and CD8$^+$ T cells, through multiple inhibitory pathways, resulting in tumor immune evasion and progression (4).

Various Treg-targeting antibodies against upregulated immune-checkpoint receptors [e.g., cytotoxic T lymphocyte (CTL)–associated antigen-4 (CTLA-4), GITR, and OX40] on intratumoral Tregs are now undergoing clinical trials as anticancer immunotherapies (2, 5, 6). Ipilimumab (Yervoy), which targets CTLA-4, is clinically approved to treat melanoma (2). In preclinical murine models, anti–CTLA-4 antibody (Ab) mediates antitumor activity via selective depletion of intratumoral Tregs through Fc-mediated Ab-dependent cellular cytotoxicity (ADCC) and cellular phagocytosis (ADCP), as well as by activation of effector T cells in the TME (7, 8). However, whether the antitumor activity of the anti–CTLA-4 Ab is achieved by affecting the number or the function of Tregs, effector T cells, or both is still controversial in human clinical settings (9–11). Nonetheless, anti–CTLA-4 Ab therapy is often associated with undesirable immune-related adverse effects (irAE), such as autoimmunity-related toxicities (12–14), although the exact mechanism is unclear. In this regard, a safer efficacious strategy of Treg-targeted anticancer therapy is to selectively inhibit Tregs only in the TME without unfavorable effects on peripheral Tregs and effector T cells, maintaining systemic immune homeostasis.

Neuropilin-1 (NRP1), a non–tyrosine kinase receptor, is a promising target for specific inhibition of intratumoral Tregs because NRP1 is expressed more frequently on intratumoral Tregs in mouse and human tumors (15, 16). NRP1 is critical for Treg function in the TME (15–17). NRP1 functions as a homodimer or as a coreceptor of vascular endothelial growth factor (VEGF) receptors (VEGFR) for VEGF ligands and Plexin for semaphorin (Sema) ligands, triggering multiple signaling pathways depending on the cellular context (18, 19). Treg surface-expressed NRP1 interacts with semaphorin 4a (Sema4A) ligand expressed on immune cells to potentiate Treg function and survival (17), and acts as a coreceptor of VEGFR2 for VEGF to stimulate Treg proliferation in mice and human (20, 21). In mouse models, Treg-restricted knockout of NRP1 reduces tumor growth (17, 21), highlighting the importance of NRP1-expressing

[1]Department of Allergy and Clinical Immunology, Ajou University School of Medicine, Suwon, Republic of Korea. [2]Department of Molecular Science and Technology, Ajou University, Suwon, Republic of Korea. [3]Department of Hematology-Oncology, Ajou University School of Medicine, Suwon, Republic of Korea. [4]Department of Otolaryngology, Ajou University School of Medicine, Suwon, Republic of Korea. [5]Department of Thoracic and Cardiovascular Surgery, Ajou University School of Medicine, Suwon, Republic of Korea.

Note: Supplementary data for this article are available at Cancer Immunology Research Online (http://cancerimmunolres.aacrjournals.org/).

Corresponding Authors: Yong-Sung Kim, Ajou University, 206 Worldcup-ro, Yeongtong-gu, Suwon 16499, Gyeonggi, Republic of Korea. Phone: 82-31-219-2662; Fax: 82-31-219-1610; E-mail: kimys@ajou.ac.kr; Seokjin Haam, Department of Thoracic and Cardiovascular Surgery, Ajou University School of Medicine, 164 Worldcup-ro, Yeongtong-gu, Suwon 16499, Republic of Korea. E-mail: haamsj@aumc.ac.kr; and Chul-Ho Kim, Department of Otolaryngology, Ajou University School of Medicine, 164 Worldcup-ro, Yeongtong-gu, Suwon 16499, Republic of Korea. E-mail: ostium@ajou.ac.kr

Cancer Immunol Res 2020;8:46–56

doi: 10.1158/2326-6066.CIR-19-0143

($NRP1^+$) Tregs in suppressing antitumor immunity. Despite these data identifying NRP1 as a potential target for intratumoral Treg-targeted therapy, agents targeting NRP1 have not been well examined.

Here, we report a strategy for the inhibition of intratumoral $NRP1^+$ Tregs by NRP1-targeting Fc(AAG)-TPP11, in which an NRP1-specific binding peptide TPP11 was fused to the C-terminus of an effector function–deficient immunoglobulin Fc(AAG) variant. We demonstrated that Fc(AAG)-TPP11 selectively inhibited NRP1-dependent Treg function and survival to boost antitumor activity in the TME of mouse models, without noticeable systemic toxicities, and suppressed the function of intratumoral $NRP1^+$ Tregs from human cancers.

Materials and Methods

Construction, expression, and purification of proteins and antibodies

To produce an effector-silent human IgG1 Fc variant, L234A/L235A/P329G mutations were introduced into the wild-type CH2 domain of IgG1 Fc (residues 225–447 in EU number) using PCR-based mutagenesis followed by subcloning into pcDNA3.4 (Thermo Fisher Scientific) to generate pcDNA3.4-Fc(AAG) [hinge-CH2(AAG)-CH3]. To produce Fc(AAG)-TPP11, the genes encoding the CH3-$(G_4S)_3$-TPP11 peptide (HTPGNSKPTRTPRR) region were cloned into pcDNA3.4-Fc(AAG), generating pcDNA3.4-Fc(AAG)-TPP11 [hinge-CH2(AAG)-CH3-$(G_4S)_3$-TPP11]. To construct the anti–CTLA-4 9D9 Ab, variable regions in the heavy chain and light chain, synthesized according to patent US 20110044953, were subcloned in-frame into pcDNA3.4-mIgG2a-heavy chain (CH1-hinge-CH2-CH3) and pcDNA3.4-mIgG2a-light chain carrying the mouse kappa constant domain sequence, respectively. A plasmid encoding the extracellular region of the Sema4A-hinge-CH2-CH3-6 × histidine tag was obtained from Addgene. All plasmids were confirmed by sequencing and purified using the NucleoBond Xtra Midi Kit (Machery Nagel) for endotoxin-free production of proteins. Fusion proteins and antibodies were expressed by transient transfection into HEK293F cells (Thermo Fisher Scientific) and purified as previously described (22).

Cell culture

The mouse colon carcinoma CT26 cell line was a kind gift from Prof. Chang-Yuil Kang in 2016 (Seoul National University, Korea). The B16/F10 murine melanoma cell line was purchased in 2016 from the Korean Cell Line Bank. Cell lines were authenticated by DNA short tandem repeat profiling (ABION CRO) in 2017, and used within 20 passages. Tumor cell lines were maintained in Dulbecco's Modified Eagle Medium containing 10% heat-inactivated fetal bovine serum (FBS; GE Healthcare, SH30084.03) and 1% penicillin–streptomycin (WelGENE). Cell lines were routinely screened for *Mycoplasma* contamination (CellSafe). Mouse Tregs and conventional $CD4^+$ T cells were cultured and/or expanded in RPMI-1640 medium (GE Healthcare, SH30027.01) supplemented with 10% heat-inactivated FBS, 100 U/mL penicillin, 100 μg/mL streptomycin, and 0.25 μg/mL amphotericin B. Human tumor-infiltrating lymphocytes (TIL) were expanded in X-VIVO 15 medium (Lonza, 04-418Q) supplemented with 15% human serum (Lonza, 4W-820).

Western blot analysis

A standard procedure for Western blotting was performed as described previously (22). Equal amounts of lysates were analyzed by Western blotting, with β-actin serving as a loading control. Band intensities were quantified using ImageJ software (22).

Mice

Four- to 5-week-old female Balb/c and C57BL/6 mice were purchased from Orient Bio. For adoptive transfer models, 4-week-old female Balb/c athymic nude mice (Orient Bio) were used. Mice were maintained according to the guidelines of the Institutional Animal Care and Use Committee of Ajou University (Suwon, Korea; approval ID: 2017-0011).

Human T-cell populations

Peripheral blood mononuclear cells (PBMC) from healthy donors ($n = 18$) as well as PBMCs, peripheral blood, and tumor tissues from patients with head and neck squamous cell carcinoma (HNSCC, $n = 20$) and non–small cell lung cancer (NSCLC, $n = 15$) were acquired under protocols approved by the Institutional Review Board of Ajou University (approval ID: AJIRB-BMR-SMP-17-194). All patients gave written informed consent before sample collection. Tumor specimens were obtained at the time of surgical resection without restrictions on cancer subtype, smoking status, age, and race. Blood was drawn in BD vacutainer (BD Biosciences, 367874). PBMCs and TILs were isolated using standard density centrifugation with Ficoll-Paque PLUS (GE Healthcare, 17-5442-03). Cells dissolved in 10% DMSO in FBS and kept in a Nalgen Cryo 1°C freezing container (Thermo Fisher Scientific, 5100-0001) were immediately transferred to a −80°C deep freezer. After 24 hours, cryopreserved cells were transferred into a liquid nitrogen tank and stored between 1 and 14 days prior to staining for NRP1 and analysis of Treg function. In some experiments, TILs were expanded *in vitro* in the presence of anti-CD3ε Ab/anti-CD28 Ab-coated beads (Thermo Fisher Scientific, 11456D), and recombinant human IL2 (hIL-2; R&D Systems, 202-IL) for 7 days.

Tumor inoculation and treatment

Balb/c mice and C57BL/6 mice were implanted subcutaneously on the right flank with 10^6 CT26 and 3×10^5 B16F10 tumor cells in 100 μL of PBS, respectively. Starting on day 12 after tumor inoculation, Fc(AAG), Fc(AAG)-TPP11, or 9D9 Ab or a PBS vehicle were intraperitoneally injected every 2 to 3 days. Tumor volumes and body weights were measured as described previously (23). Tumor growth inhibition (TGI) was determined on the last day of the study according to the formula: $TGI\ (\%) = (100 - (V_f^{Fc(AAG)\text{-}TPP11} - V_i^{Fc(AAG)\text{-}TPP11})/(V_f^{Fc(AAG)} - V_i^{Fc(AAG)}) \times 100)$, where V_i was the initial mean tumor volume and V_f was the final mean tumor volume in the Fc(AAG)-TPP11 or Fc(AAG) treatment group, as indicated by the superscript notation (23). The mice were sacrificed by CO_2 asphyxiation, and in some cases, tumors, spleens, and tumor-draining lymph nodes (tdLN) were harvested for *ex vivo* analysis. For rechallenge analysis, Balb/c mice that were free of CT26 tumors as a result of treatment with Fc(AAG)-TPP11 or 9D9 Ab, along with age-matched naïve control mice, were rechallenged subcutaneously in the opposite flank with 10^6 CT26 cells 10 weeks after the initial CT26 tumor challenge as described above.

Adoptive transfer of Tregs into Balb/c nude mice

$CD4^+CD25^+$ Tregs and $CD8^+$ T cells were purified by flow cytometry using a FACSAria III system (BD Biosciences) from the tdLN and spleen of day −21 CT26-bearing Balb/c mice. Tregs were further expanded *in vitro* in 24-well plate in the presence of anti-CD3ε Ab/anti-CD28 Ab–conjugated latex beads and hIL-2 for 7 days. Balb/c

nude mice were implanted subcutaneously in the right flank with 10^6 CT26 tumor cells on day 0 as described above and intravenously injected with expanded Tregs (5×10^6) and/or $CD8^+$ T cells (5×10^6) in 100 μL PBS on day 5. When the mean tumor volume reached 120 to 150 mm^3 (day 7), Fc(AAG), Fc(AAG)-TPP11, or PBS vehicle control were i.p. injected at 10 mg/kg in a total volume of 200 μL every 3 days. Tumor volumes were measured twice per week.

In vitro suppression assays of Tregs and Transwell suppression assay

$CD4^+CD25^+CD39^+$ Tregs from the spleen and tdLN cells of CT26 tumor–bearing mice (TBM) or conventional $CD4^+CD25^-$ T cells (Tconv) from the spleen and lymph nodes of naïve Balb/c mice were purified using a FACSAria III system (BD Biosciences). For the *in vitro* suppression assay, Tregs (5×10^4) were cultured with Tconvs (2×10^5) in a 96-well plate at a 1:4 ratio in the presence of anti-CD3ε Ab/anti-CD28 Ab–conjugated latex beads (1:1 ratio), 2 μmol/L agents [Fc(AAG), Fc(AAG)-TPP11, or 9D9 Ab] for 3 days. Proliferation of Tconvs was measured using the CellTiter-Glo (CTG) assay (Promega, G7570), according to the manufacturer's protocol. The luminescence was measured by means of the Cytation 3 imaging multimode reader (Biotek). The percentage of suppressive function of Tregs was calculated according to the following formula: Suppression (%) = [1 − L (Tregs + Tconvs)/L(Tconvs only)] × 100, where L(Tregs + Tconvs) stands for the luminescence of Tconvs cocultured with Tregs and L (Tconvs only) stands for the luminescence of Tconvs without Tregs under the indicated conditions (15). Cytokine concentration in the supernatants was determined using an ELISA Ready-SET-GO kit (Thermo Fisher Scientific). Absorbance was read at 450 nm on the Cytation 3 imaging multimode reader. For the suppression assay of human Tregs, $CD4^+CD25^{hi}$ Tregs were used because only $CD4^+CD25^{hi}$ human T cells constitutively express Foxp3 and reproducibly suppress human Tconvs (24). For Transwell suppression assay, Tregs (1.25×10^4) were stimulated with anti-CD3ε Ab/anti-CD28 Ab–conjugated latex beads (1:1 ratio) in the presence of Sema4A-Fc- or Fc-conjugated latex beads (1:1 ratio), and/or 2 μmol/L of agents [Fc(AAG) or Fc(AAG)-TPP11] in the top chamber of a Millipore Millicell 24 (0.4 mm pore size). In the bottom well, Tconvs (5×10^4) were stimulated with anti-CD3ε Ab/anti-CD28 Ab–conjugated latex beads (5×10^4). After 3 days of culture, the levels of IL2 and IL10 in the supernatants of the bottom wells were determined using the ELISA Ready-SET-GO kit.

Liver enzymes activity assay

The levels of alanine aminotransferase (ALT) and aspartate aminotransferase (AST) in blood serum obtained at 24 hours after the last treatment with the indicated agents were measured using transaminase kits (AM102-K for ALT and AM103-K for AST; Asan Pharmaceutical Co.) according to the manufacturer's instructions.

Immunofluorescence microscopy of cells

To detect colocalization of NRP1/Fc(AAG)-TPP11 on Tregs, flow cytometrically purified Tregs ($CD4^+CD25^+CD39^+$, 5×10^4 cells) from tdLN cells of day 24 CT26-TBM were attached to coverslips in 24-well culture plates. The cells were treated with 2 μmol/L of Fc(AAG)-TPP11 or Fc(AAG) for 1 hour at 37°C, and immunofluorescence staining was performed as previously described (22, 25). Center-focused single z-section images were obtained on a Zeiss LSM710 system with ZEN software (Carl Zeiss). When a 40 × objective lens was used, zoom factor 2 was applied to improve the resolution.

Flow cytometry

Single-cell suspensions were prepared by mechanically dissociating the tumors, tdLNs, or spleens through a 70-μm wire-mesh screen. For flow cytometry analysis, monoclonal antibodies specific for CD45 (clone 30-F11), CD3ε (clone 145-2C11 for mouse), CD8α (clone 53-6.7), CD4 (clone GK1.5 for mice and clone RPA-T4 for human), CD25 (clone PC61.5 for mice and clone BC96 for human), CD39 (clone 24DMS1), NRP1 (clone 3DS304M for mice and clone TNKU-SOHA for human), VEGFR2 (clone Avas12a1), CD73 (clone TY/11.8), CTLA-4 (clone UC10-4B9), PD-1 (clone J43), granzyme B (clone NGZB), IFNγ (clone XMG1.2), IL2 (clone JES6-5H4), TNFα (clone TN3-19.12), IL10 (clone JES5-16E3), Ki-67 (clone solA15), Foxp3 (clone FJK-16s), and the isotype control antibodies (rat IgG1, rat IgG2a, and rat IgG2b) were purchased from Thermo Fisher Scientific. Surface staining was performed at 4°C with antibodies resuspended in PBS with 2% FBS and 2 mmol/L EDTA. For intracellular cytokine staining, cells were activated with phorbol 12-myristate 13-acetate (100 ng/mL) plus ionomycin (500 ng/mL) or cell lysates in a humidified incubator with 5% CO_2 at 37°C for 16 hours. Next, Brefeldin A (BD Biosciences, 00-4506-51) was added for the final 6 hours of culture to prevent protein transport from the endoplasmic reticulum to the Golgi apparatus. All intracellular staining and Foxp3 staining were performed using a BD cytofix/cytoperm kit (BD Biosciences, 554714) and Foxp3/transcription factor staining buffer set (Thermo Fisher Scientific, 00-5523-00), respectively. Fluorescence-activated cell sorting (FACS) data were acquired using the FACSAria III and analyzed with FlowJo software (Tree Star).

Statistical analysis

Statistical analyses were conducted using GraphPad Prism software (GraphPad, Inc.). Data are presented as the mean ± SEM for pooled data or ± SD for representative data from at least three independent experiments, unless otherwise specified. One-way analysis of variance (ANOVA) with the Newman–Keuls *post hoc* test was used to evaluate the significance of differences. In performing statistical tests, no correction was made. *P* values less than 0.05 were considered statistically significant. *P* values less than 0.05, 0.01, and 0.001 are indicated as *, **, and ***, respectively, in each figure.

Results

Fc(AAG)-TPP11 inhibited Tregs by downregulating NRP1 and blocking NRP1 function

We previously generated a human immunoglobulin IgG1 Fc-fused NRP1-binding peptide TPP11, Fc-TPP11, which specifically binds to the ligand binding site of NRP1 with approximately 28 nmol/L affinity (22, 25). This blocks the binding of ligands such as VEGF and Sema to NRP1 (22, 25). Fc-TPP11 cross-reacts equivalently with mouse NRP1 (25) because mouse and human NRP1 share high sequence homology (93%), with 100% conservation of the TPP11-binding pocket in NRP1 (26). To silence Fc-mediated effector functions, we introduced L234A, L235A, and P329G mutations, known as LALAPG (27, 28), into the Fc region, generating Fc(AAG)-TPP11 (**Fig. 1A**). The LALAPG mutation completely abolishes Fc(AAG) binding to Fcγ receptors and complements while retaining the typical pharmacokinetics in mice (27, 28). Thus, we hypothesized that Fc(AAG)-TPP11 would not deplete $NRP1^+$ cells through effector functions such as ADCC and ADCP as well as complement-dependent cytotoxicity. As a surrogate Ab of the clinically approved anti–CTLA-4 ipilimumab, we used antimurine CTLA-4 9D9 Ab with the mouse IgG2a isotype, which elicits the most effective antitumor

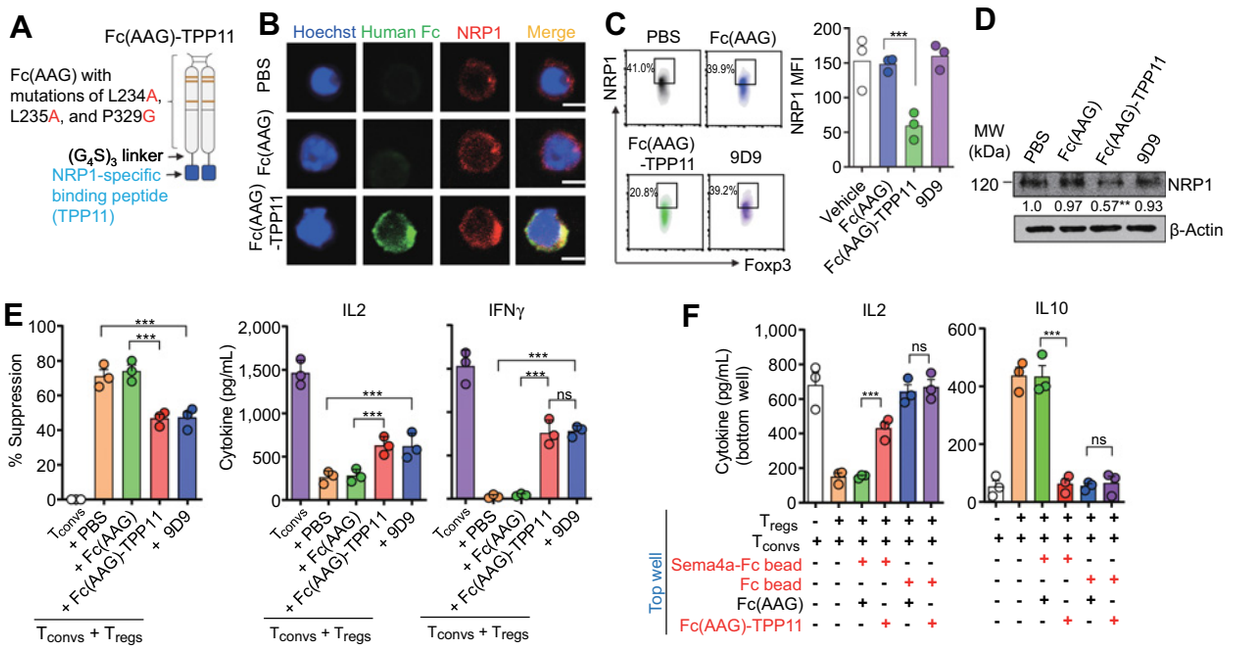

Figure 1.

Fc(AAG)-TPP11 inhibited Treg function by downregulating NRP1 and blocking the NRP1–Sema4A axis. **A,** Schematic representation of Fc(AAG)-TPP11. **B,** Binding specificity of Fc(AAG)-TPP11 (green) to Treg-surface expressed NRP1 (red), as determined by confocal fluorescence microscopy. Nuclei were costained with Hoechst 33342 (blue). Scale bars, 20 μm. Representative images from three independent experiments. Representative flow cytometric analysis (**C**) and Western blots (**D**) showing cell surface and total cell expression levels of NRP1 on Tregs, respectively, after treatment with 2 μmol/L of Fc(AAG)-TPP11, Fc(AAG), or 9D9 Ab for 1 hour at 37°C. **C**, Right, quantification of NRP1 expression on the Tregs by mean fluorescence intensity (MFI). **D,** The number below the panel indicates the relative mean value ($n = 2$) of band intensity to that of PBS-treated control after normalization of the band intensity to that of β-actin. **E,** Effects of the indicated agents (2 μmol/L) on Treg-suppressive function against $CD4^+CD25^-$ Tconvs, with the readout being Tconv proliferation by CTG assays as well as IL2 and IFNγ secretion from Tconvs by ELISA. **F,** Effects of the indicated agents (2 μmol/L) on the suppressive function of Tregs in the top well against Tconvs in the bottom well, with the readout of IL2 and IL10 in the bottom well by ELISA. $CD4^+CD25^+CD39^+$ Tregs (**B–F**) from tdLN of day 24 CT26-TBM and $CD4^+CD25^-$ Tconvs (**E** and **F**) of MHC-matched naïve Balb/c mice were purified by flow cytometry. Indicated cell subsets were defined by the gating strategy shown in Supplementary Fig. S7. **C, E,** and **F,** Each symbol represents the value obtained from individual mice. Data represent the mean ± SEM. Statistical analysis was performed using one-way ANOVA, followed by the Newman–Keuls *post hoc* test. **D,** **, $P < 0.01$ versus PBS-treated control. **C, E,** and **F,** ***, $P < 0.001$ between the indicated groups; ns, not significant.

activity by depleting Tregs mainly through Fc-mediated effector functions (7).

For *in vitro* analysis, $CD4^+CD25^+CD39^+$ Tregs were purified by flow cytometry from tdLNs of Balb/c mice bearing syngeneic CT26 colon carcinoma as previously performed (29). Confocal microscopic analysis revealed that Fc(AAG)-TPP11, but not Fc(AAG), colocalized with NRP1 on Treg plasma membrane (**Fig. 1B**), indicating specific binding of Fc(AAG)-TPP11 to Treg-surface expressed NRP1. Treatment of Fc(AAG)-TPP11 at 37°C for 1 hour, but not Fc(AAG) and anti–CTLA-4 9D9 Ab, dramatically reduced the cell surface and total cell expression levels of NRP1 on Tregs (**Fig. 1C** and **D**). These data suggest that Fc(AAG)-TPP11 downregulated NRP1 on Tregs by triggering cellular internalization, as observed in cancer cell–expressed NRP1 (22).

To evaluate the impact of Fc(AAG)-TPP11 on Treg activity *in vitro*, Tconvs from the spleen of naïve Balb/c mice were cocultured with tdLN-derived Tregs in the presence and absence of Fc(AAG)-TPP11. The effect was monitored by the suppression of Tconvs proliferation and secretion of IL2 and IFNγ. Unlike Fc(AAG), Fc(AAG)-TPP11 significantly blocked the suppressive activity of Tregs at a comparable level to anti–CTLA-4 9D9 Ab (**Fig. 1E**). The effect of Fc(AAG)-TPP11 was likely dependent on $NRP1^+$ Tregs because NRP1 was specifically expressed on $CD4^+Foxp3^+$ Tregs, but not on $CD4^+Foxp3^-$ Tconvs in C57BL/6 mice (21) and Balb/c mice (Supplementary Fig. S1A). In contrast, anti–CTLA-4 9D9 affected both Tconvs and Tregs (30). A previous study showed that ligation of Sema4A to NRP1 on Tregs potentiates Treg function by enhancing soluble suppressive molecules such as IL10 (17). To determine whether Fc(AAG)-TPP11 limits Treg function by blocking the Sema4A-NRP1 axis, we performed a Transwell suppression assay. Indeed, Fc(AAG)-TPP11 reduced the suppressive function of Tregs stimulated with Sema4A-bead in the top chamber of a Transwell plate against the proliferation of Tconvs in the bottom chamber, as determined by the decreased secretion of IL10 by Tregs and increased IL2 secretion by Tconvs (**Fig. 1F**). These results indicated that Fc(AAG)-TPP11 inhibited Treg function by downregulating NRP1 on the Treg surface and blocking the interactions between Treg-expressed NRP1 and its stabilizing ligand Sema4a.

Fc(AAG)-TPP11 elicited potent *in vivo* antitumor effects

We next evaluated the *in vivo* antitumor efficacy of Fc(AAG)-TPP11 in comparison with 9D9 Ab in immunocompetent Balb/c mice bearing syngeneic CT26 colon carcinoma and C57BL/C mice bearing syngeneic B16F10 melanoma. B16F10 cells expressed NRP1 on the cell surface, whereas CT26 cells did not (Supplementary Fig. S1B). After

randomization of mice with similar baseline tumor volumes (~120–150 mm^3) on day 12 after tumor cell inoculation, Fc(AAG)-TPP11 and Fc(AAG) were administered at a dose of 10 mg/kg every 2 days by i.p. injection for a total of 6 doses (**Fig. 2A**). In a separate cohort of mice, the anti–CTLA-4 9D9 Ab was i.p. injected at a dose of 2.5 mg/kg every 3 days for a total of 4 doses because the IgG2a Ab has a longer serum half-life than Fc-fused proteins (7, 25). Compared with the vehicle or Fc(AAG) control, Fc(AAG)-TPP11 significantly delayed tumor growth with TGI of 72.4% and 74.3% for CT26 and B16F10 tumors, respectively, on day 24 after tumor inoculation, regardless of NRP1 expression on cancer cells (**Fig. 2B** and **C**; Supplementary Fig. S2). When we monitored tumor growth after the cessation of therapy, F (AAG)-TPP11 resulted in an 80% and 50% of the long-term survival of CT26- and B16F10-TBM, respectively (**Fig. 2B** and **C**). Treatment of anti–CTLA-4 9D9 Ab with the murine IgG2a constant region exhibited potent antitumor activity in both models, in line with previous results (7). Notably, the antitumor effect of Fc(AAG)-TPP11 was just as potent as the 9D9 Ab (**Fig. 2B** and **C**; Supplementary Fig. S2). During Fc(AAG)-TPP11 therapy, no weight loss (**Fig. 2D**), diarrhea, or death of TBM or any substantial elevations in liver enzymes (ALT and AST) in the blood were observed (**Fig. 2E** and **F**), indicating no significant Fc(AAG)-TPP11–induced systemic toxicity. However, 9D9 Ab treatment slightly elevated liver enzyme levels (**Fig. 2E** and **F**) and caused a 20% mortality rate ($n = 5/25$) in B16F10-TBM (Supplementary Fig. S2B), reflecting the minor toxicities, in accordance with previous findings (31). These data demonstrate the potent antitumor

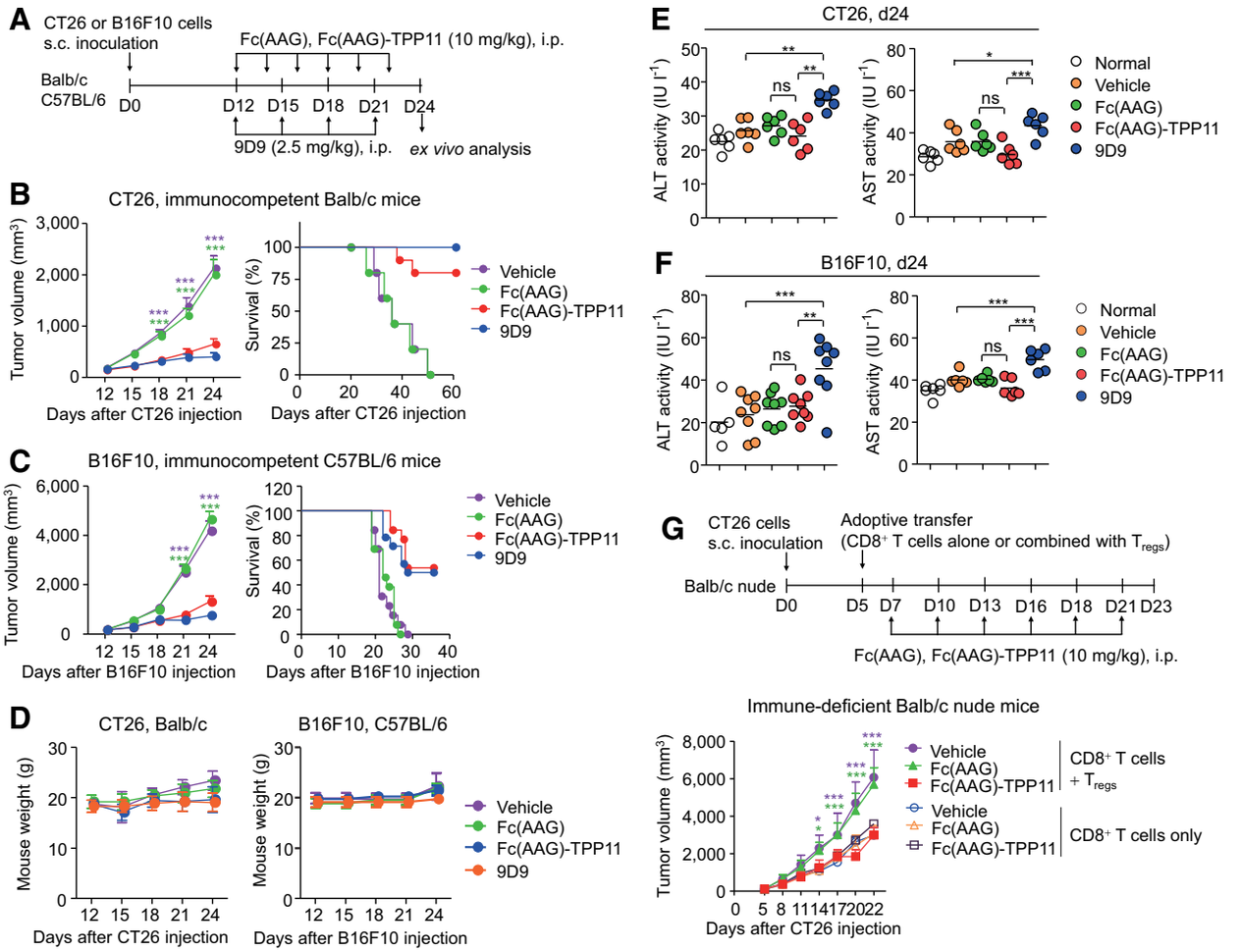

Figure 2.

Fc(AAG)-TPP11 elicited antitumor effects by inhibiting Tregs without systemic toxicity *in vivo*. **A,** Treatment scheme of CT26- and B16F10-TBM initiated at the tumor volume of ~120 to 150 mm^3 with either i.p. injection of Fc(AAG) or Fc(AAG)-TPP11 proteins (10 mg/kg) every 2 days or i.p. injection of 9D9 Ab (2.5 mg/kg) every 3 days. The arrows indicate each time point for treatment or assay. **B** and **C,** Tumor growth, as measured by tumor volume during treatment (left), and survival curves (right) of CT26-TBM (**B**) and B16F10-TBM (**C**) treated as described in **A**. **D,** Body weight of CT26- and B16F10-TBM during treatment. Serum levels of liver enzymes (ALT and AST) measured at day 24 in CT26-TBM (**E**) and B16F10-TBM (**F**). Each symbol represents 1 mouse; midlines indicate the mean. **G,** Adoptive transfer of $CD8^+$ T cells alone or combined with Tregs into CT26 tumor–bearing T cell–deficient Balb/c nude mice to analyze the effect of Fc(AAG)-TPP11 on *in vivo* functionality of Tregs. **B–D** and **G,** Symbols and error bars represent the mean ± SEM. Data pooled from five independent experiments at least with 5 mice/group (**B–D**; $n = 25$) or one representative experiment for 8 mice/group (**G**). Significance was tested using one-way ANOVA followed by the Newman–Keuls *post hoc* test. *, $P < 0.05$; **, $P < 0.01$; ***, $P < 0.001$ versus the Fc(AAG)-TPP11–treated TBM (**B** and **C**), between the indicated groups (**E** and **F**), or versus Fc(AAG)-treated mice transferred with $CD8^+$ T cells only (**G**); ns, not significant.

effect of Fc(AAG)-TPP11, which was comparable with that of the Treg-depleting anti–CTLA-4 Ab (7), in two mouse syngeneic tumor models without systemic toxicity.

Fc(AAG)-TPP11 inhibited the suppressive function of Tregs against CD8$^+$ T cells

To examine whether the *in vivo* antitumor effect of Fc(AAG)-TPP11 is directly attributed to inhibition of NRP1$^+$ Tregs, we evaluated the impact of Fc(AAG)-TPP11 on Tregs-dependent inhibition of CD8$^+$ T cell–mediated antitumor immunity in T cells-deficient Balb/c nude mice. To prepare effector CD8$^+$ T cells and Tregs against CT26 tumors, we isolated CD8$^+$ T cells and CD4$^+$CD25$^+$ Tregs from the spleen and tdLN of CT26-bearing immunocompetent Balb/c mice on day 21 after tumor inoculation (32). We further expanded Tregs *in vitro* for adoptive transfer. The expanded Tregs did not differ from fresh Tregs in the surface expression of NRP1 (Supplementary Fig. S3A) and the *in vivo* suppressive effects on CD8$^+$ T cell–mediated TGI in CT26 tumor–bearing Balb/c nude mice (**Fig. 2G**; Supplementary Fig. S3B). The lack of significant differences in NRP1 expression between fresh and expanded Tregs is consistent with a previous study (33). To evaluate the inhibition specificity of Fc(AAG)-TPP11 for NRP1$^+$ Tregs, CT26 tumor–bearing Balb/c nude mice were adoptively transferred with CD8$^+$ T cells alone or combined with expanded Tregs and then the agents were intraperitoneally injected every 3 days for a total of 6 doses (**Fig. 2G**). Fc(AAG)-TPP11 treatment, but not vehicle and Fc(AAG), resulted in delayed tumor growth in mice cotransferred with both CD8$^+$ T and Tregs at a comparable level to that in mice transferred with only CD8$^+$ T cells (**Fig. 2G**). These results show that Fc(AAG)-TPP11 specifically interferes with the suppressive function of NRP1$^+$ Tregs against the antitumor immunity of CD8$^+$ T cells.

Fc(AAG)-TPP11 reduced Treg function to cause unstable phenotypes in the TME

To examine functional changes of intratumoral Tregs by Fc(AAG)-TPP11, we isolated Tregs from tumor tissues of day 24 CT26- and B16F10-TBM treated as described in **Fig. 2A** and cocultured these cells with CD4$^+$CD25$^-$ Tconvs isolated from the respective naïve mice. Intratumoral Tregs from Fc(AAG)-TPP11– or 9D9 Ab–treated TBM exhibited a significantly attenuated capacity to inhibit the proliferation of Tconvs compared with those from vehicle- and Fc(AAG)-treated TBM (**Fig. 3A**). To further investigate the mechanism of *in vivo* inhibition of Treg function by Fc(AAG)-TPP11, we determined the NRP1 surface levels of Tregs by flow cytometry. Fc(AAG)-TPP11 selectively reduced NRP1 expression on intratumoral Tregs, with no impact on spleen-derived Tregs, in both CT26- and B16F10-TBM (**Fig. 3B**). This tumor site–specific effect of Fc(AAG)-TPP11 may be attributed to selective upregulation of NRP1 on intratumoral Tregs compared with that in tdLN- and spleen-derived Tregs (Supplementary Fig. S4A and S4B). Notably, Fc(AAG)-TPP11 did not affect the expression of CTLA-4 and PD-1 (Supplementary Fig. S4C and S4D), revealing the NRP1-targeting specificity. We further observed that Fc (AAG)-TPP11 or 9D9 Ab treatment significantly reduced the frequency of intratumoral IL10$^+$ and CD73$^+$ (ecto-5′-nucleotidase) Tregs relative to vehicle and Fc(AAG) treatments in both CT26- and B16F10-TBM (**Fig. 3C** and **D**). The effect of Fc(AAG)-TPP11 was consistent with the phenotypes previously observed in NRP1-deficient Tregs (15, 17, 34).

In mice, Treg-specific genetic deletion of NRP1 causes Tregs to produce IFNγ, undermining the function of surrounding wild-type Tregs to boost antitumor immunity (15). When we analyzed intratumoral Tregs from day 24 CT 26- and B16F10-TBM, Fc(AAG)-TPP11 elevated the frequency of intratumoral IFNγ$^+$ Tregs in both TBM (**Fig. 3E**). Given that NRP1 expression is linked to Foxp3 expression (35), we further analyzed the intensity of Foxp3 expression in intratumoral Tregs. We found that Fc(AAG)-TPP11 treatment significantly decreased Foxp3 expression only in intratumoral Tregs, but not in peripheral Tregs from the spleen, in both TBM (**Fig. 3F**), indicating that NRP1 downregulation in Tregs reduced Foxp3 expression. Thus, NRP1-downregulated intratumoral Tregs by Fc(AAG)-TPP11 displayed the typical unstable Treg phenotypes including reduced Foxp3 expression and enhanced production of proinflammatory IFNγ (36, 37). These results suggested that Fc(AAG)-TPP11 specifically limits intratumoral Treg function by downregulation of NRP1 on the surface, thereby causing Tregs to have unstable phenotypes in the TME. Anti–CTLA-4 9D9 Ab treatment also exhibited tumor site–specific reduction in Foxp3 expression for intratumoral Tregs, but not for splenic Tregs (**Fig. 3F**), explaining the attenuated functionality of intratumoral Tregs in both TBM (**Fig. 3A** and **C–E**).

Fc(AAG)-TPP11 promoted antitumor immunity in the TME

Intratumoral Tregs exhibit higher proliferative activity than peripheral Tregs (38), but NRP1-deficient Tregs show compromised survival and proliferation (17). Based on the preferential expression of VEGFRs, NRP1 and VEGFR2, on intratumoral Tregs compared with that on peripheral Tregs from the spleen and tdLN (Supplementary Fig. S4E), we hypothesized that rather than blocking the migration of Tregs into tumors, Fc(AAG)-TPP11 limited the proliferation of intratumoral Tregs, thereby reducing the frequency of Tregs in the TME. Indeed, Fc(AAG)-TPP11 treatment significantly reduced the expression of Ki-67, a proliferation marker, in intratumoral Tregs (**Fig. 4A**) and decreased the frequency of intratumoral Tregs in CT26- and B16F10-TBM, compared with vehicle or Fc(AAG) treatment (**Fig. 4B**). Such effects of Fc(AAG)-TPP11 were restricted to tumor sites, with no impact on the tdLN and spleen of both TBM (**Fig. 4A** and **B**); these data were consistent with the selective NRP1 downregulation in intratumoral Tregs by Fc(AAG)-TPP11 (**Fig. 3B**). These data suggested that the antitumor effect of Fc(AAG)-TPP11 was attributed not only to the direct suppression of intratumoral NRP1$^+$ Treg function but also to the reduced proliferation of Tregs in the TME. Anti–CTLA-4 9D9 Ab treatment also substantially reduced the proliferation and frequency of Tregs at the tumor sites with a negligible impact on peripheral Tregs in both TBM (**Fig. 4A** and **B**), in line with previous results (8).

The increased accumulation of effector T cells relative to Tregs in the TME is associated with favorable antitumor responses in mouse tumor models (2, 6, 7). To understand how NRP1 blockade of Tregs by Fc(AAG)-TPP11 exerted antitumor activity, we assessed the frequency of CD45$^+$CD3$^+$CD8$^+$ T cells (CD8$^+$ T cells) and CD45$^+$CD3$^+$CD4$^+$Foxp3$^-$ T cells (CD4$^+$Foxp3$^-$ T cells) from tumor, tdLN, and spleen of day 24 CT26- and B16F10-TBM. Fc(AAG)-TPP11 caused a significant increase in the frequency of CD8$^+$ and CD4$^+$Foxp3$^-$ T cells (**Fig. 4C**; Supplementary Fig. S5A), resulting in an augmented ratio for both CD8$^+$ and CD4$^+$Foxp3$^-$ T cells to Tregs in the TME, as observed for anti–CTLA-4 9D9 Ab treatment (**Fig. 4D**; Supplementary Fig. S5B). Fc(AAG)-TPP11 elevated the percentage of Ki-67–expressing CD8$^+$ and CD4$^+$Foxp3$^-$ TILs, but not in the cells from tdLN and spleen, compared with those observed in the vehicle or Fc(AAG) control in both TBM (**Fig. 4E**; Supplementary Fig. S5C). Intratumoral Tregs induce a dysfunctional state in CD8$^+$ TILs characterized by insufficient release of cytotoxic granules and low expression of effector cytokines (39). We observed that Fc(AAG)-TPP11

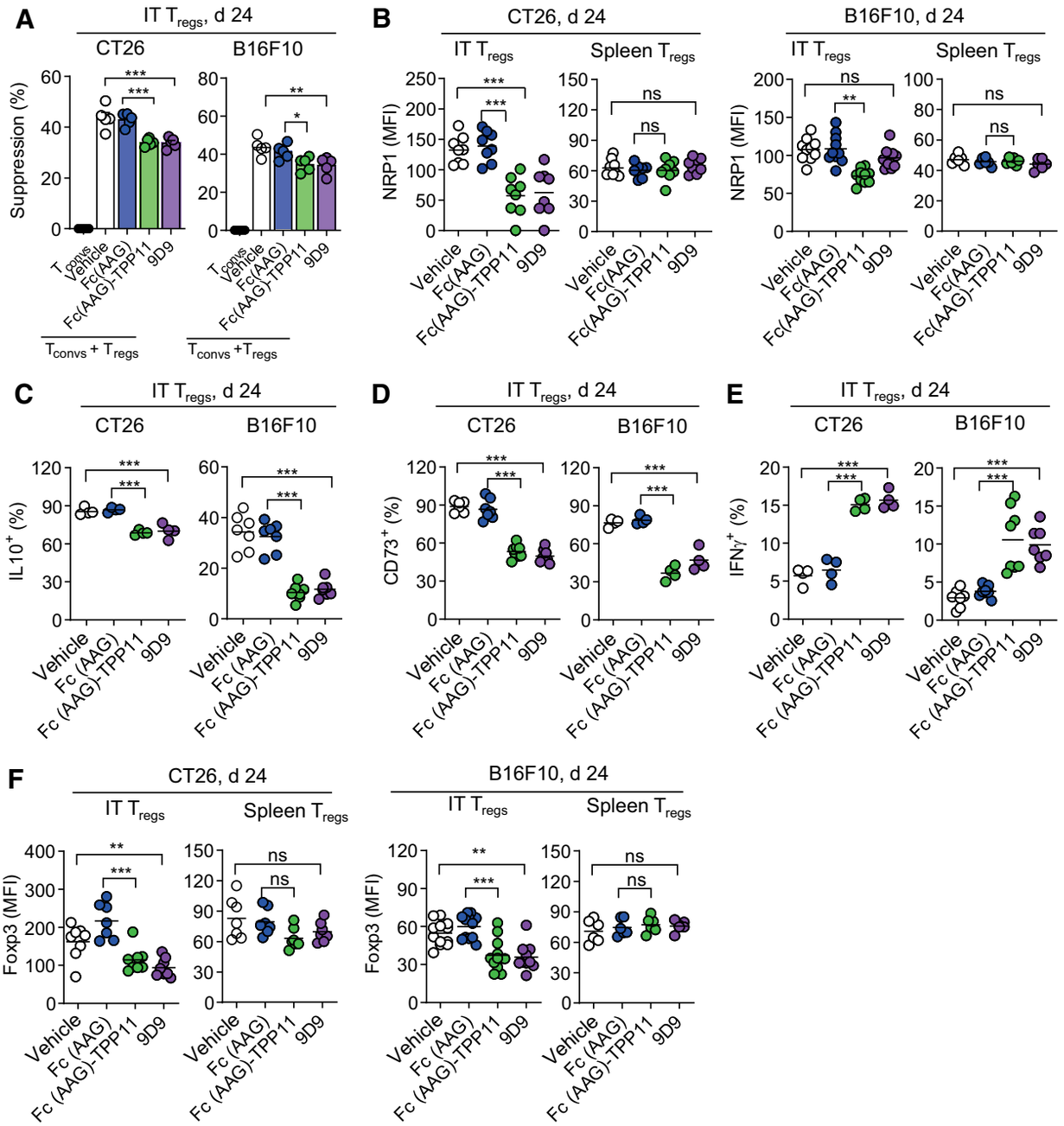

Figure 3.

Fc(AAG)-TPP11 impeded intratumoral Treg function and fostered unstable Tregs in the TME. $CD4^+CD25^+$ Tregs from tumor and/or spleen of day 24 CT26-TBM and B16F10-TBM treated as described in **Fig. 2A** were purified (**A**) or analyzed (**B–F**) by flow cytometry. Indicated cell subsets were defined by the gating strategy shown in Supplementary Fig. S7. **A,** Suppressive function of the purified intratumoral Tregs on the proliferation of Tconvs from MHC-matched naïve mice, analyzed by CTG assays after coculture at 1:4 ratio for 3 days. Percentage of suppression was calculated as described in Materials and Methods. Bars and error bars represent the mean ± SEM of three independent experiments. **B,** NRP1 expression on the surface of Tregs. Percentages of IL10-producing cells (**C**), CD73-expressing cells (**D**), or IFNγ-producing cells (**E**) among IT Tregs. **F,** Foxp3 expression in Tregs. **B** and **F,** Flow-cytometric data represented by mean fluorescence intensity (MFI). **B–F,** Each symbol represents the value obtained from individual mice; midlines indicate the mean. **A–F,** Significance was tested using one-way ANOVA followed by the Newman–Keuls *post hoc* test. *, $P < 0.05$; **, $P < 0.01$; ***, $P < 0.001$ between the indicated groups; ns, not significant. IT, intratumoral.

treatment elevated the expression of granzyme B in $CD8^+$ TILs (**Fig. 4F**) and enhanced the frequency of IFNγ-, IL2-, TNFα-expressing $CD8^+$ and $CD4^+Foxp3^-$ effector T cells from tumors, but not from tdLN and spleen, compared with those observed in vehicle and Fc (AAG) controls (**Fig. 4G**). These tumor site–specific effects of Fc (AAG)-TPP11 suggest that Fc(AAG)-TPP11 enhanced the

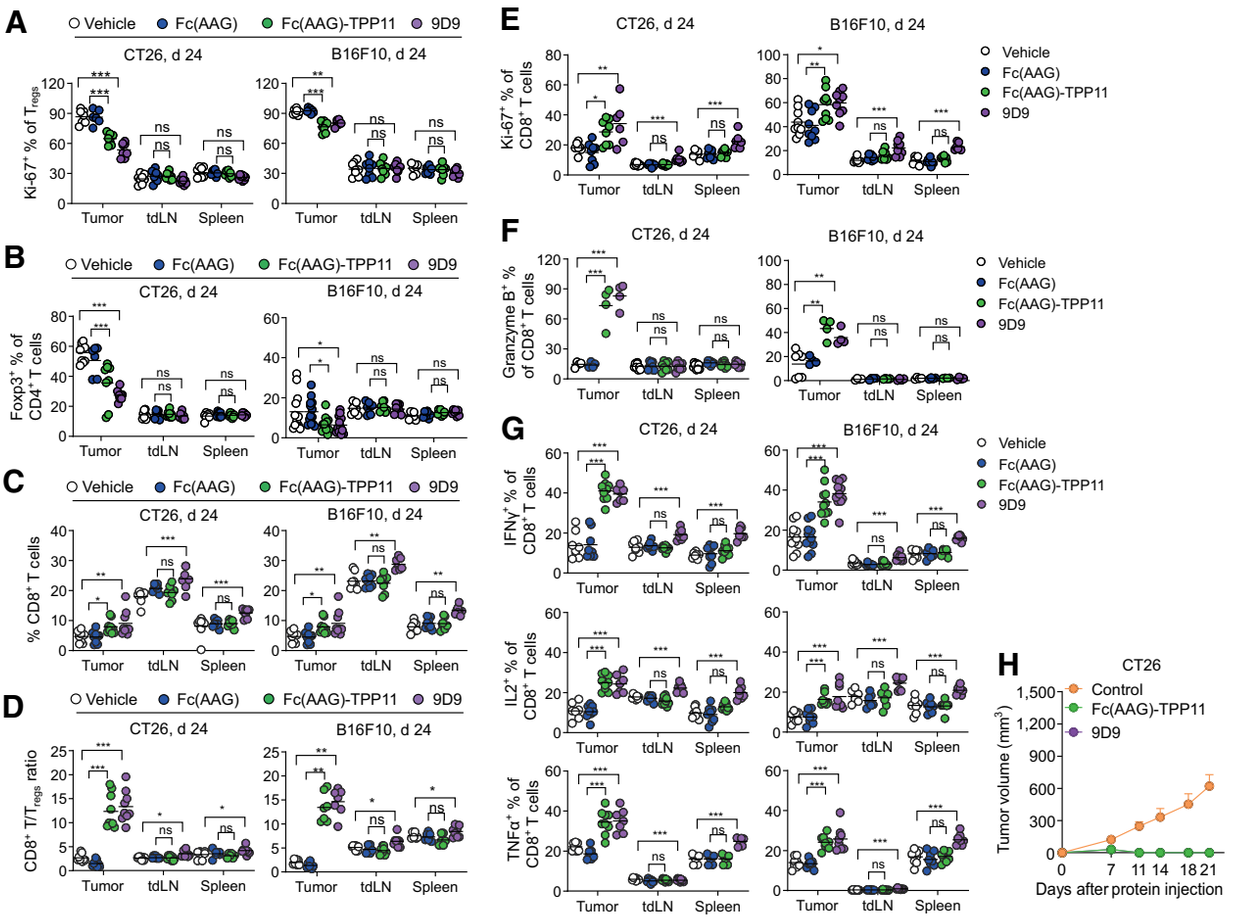

Figure 4.

Fc(AAG)-TPP11 reduced Treg proliferation and increased functional CD8$^+$ T cells in tumor. CD4$^+$CD25$^+$ Tregs and CD8$^+$ T cells from tumor, tdLN, and spleen of day 24 CT26- and B16F10-TBM treated as described in **Fig. 2A** were analyzed by flow cytometry. Indicated cell subsets were defined by the gating strategy shown in Supplementary Fig. S7. **A,** Percentage of Ki-67–expressing cells among Tregs. **B,** Percentage of Foxp3$^+$ cells among total CD4$^+$ T cells. Percentage of CD8$^+$ T cells (**C**) and ratio of CD8$^+$ T cells to Tregs (**D**). Percentage of Ki-67–expressing (**E**), granzyme B–expressing (**F**), and IFNγ-, IL2-, and TNFα-expressing (**G**) cells among CD8$^+$ T cells. **A–G,** Each symbol represents the value obtained from individual mice; midlines indicate the mean. Significance was tested using one-way ANOVA, followed by the Newman–Keuls *post hoc* test. *, $P < 0.05$; **, $P < 0.01$; ***, $P < 0.001$ between the indicated groups; ns, not significant. **H**, Mice that were tumor free of CT26 tumor by Fc(AAG)-TPP11 or 9D9 treatment as described in **Fig. 2A** were rechallenged with 10^6 CT26 cells 10 weeks after the initial CT26 tumor challenge. Tumor growth of rechallenged mice ($n = 8$) was compared with that of treatment-naïve mice ($n = 8$). Symbol and error bars represent the mean ± SEM.

proliferation and functionality of CD8$^+$ and CD4$^+$Foxp3$^-$ T cells by inhibiting the function and proliferation of NRP1$^+$ Tregs in the TME, leading to increases in the ratio of effector T cells to Tregs among TILs and antitumor immunity. In contrast, the anti–CTLA-4 9D9 Ab exhibited somewhat systemic effects on effector T cells, as it increased the frequency and functionality of both CD8$^+$ and CD4$^+$Foxp3$^-$ T cells in tdLN and spleen as well as in tumor tissues, although the magnitude of the impact was much higher in tumors than in tdLN and spleen (**Fig. 4C–E** and **G**; Supplementary Fig. S5; refs. 7, 40).

Prompted by the induction of effector T cells by Fc(AAG)-TPP11, we next determined whether Fc(AAG)-TPP11 could generate tumor-specific memory CD8$^+$ T cells in the CT26 tumor mouse model. Fc(AAG)-TPP11–treated long-term surviving mice (**Fig. 2B**) rejected a rechallenge with 10^6 CT26 cells 10 weeks after the initial tumor inoculation (**Fig. 4H**). The tumor rejection to the secondary challenge was also observed for 9D9-treated tumor-free mice (**Fig. 4H**), consistent with previous results (41, 42). These data suggest that, like the anti–CTLA-4 9D9 Ab, Fc(AAG)-TPP11 treatment generates protective memory CD8$^+$ T cells.

Human intratumoral Tregs expressed NRP1 and are inhibited by Fc(AAG)-TPP11

To determine the clinical relevance of our results, we measured NRP1 expression on blood circulating and intratumoral Tregs from patients with HNSCC and NSCLC. Given that only CD4$^+$CD25^{high} Tregs constitutively express Foxp3 and reproducibly suppress Tconvs (24), we analyzed NRP1 expression by flow cytometry on the surface of CD4$^+$CD25^{high} Tregs in PBMCs and TILs from cancer surgical resection specimens (**Fig. 5A**). In line with a previous report (15), very few human Tregs in PBMCs from healthy donors expressed NRP1 (**Fig. 5B**). Additionally, the frequency of NRP1-expressing Tregs from the PBMCs of HNSCC and NSCLC patients was negligible, as observed in the PBMCs of healthy donors (**Fig. 5B**). In contrast, substantial portions of intratumoral Tregs express NRP1

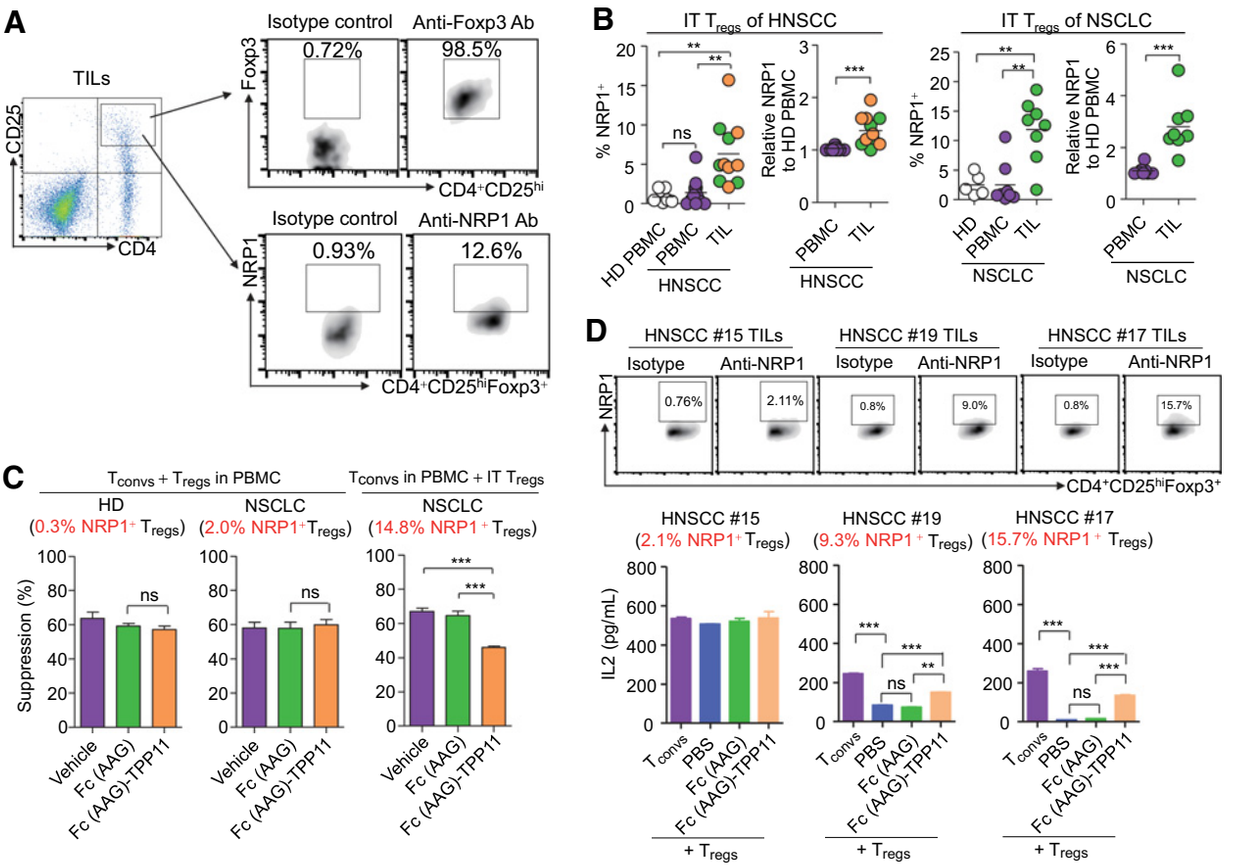

Figure 5.

Selective NRP1 expression on intratumoral Tregs from human cancers and inhibition of NRP1$^+$ Tregs by Fc(AAG)-TPP11. CD4$^+$CD25^{hi}Foxp3$^+$ Tregs and CD4$^+$CD25$^-$ Tconvs purified flow cytometrically from PBMCs of heathy donors (HD, $n = 16$) or from PBMCs and TILs of NSCLC ($n = 11$) and HNSCC patients ($n = 16$) were subjected to the following assays. Gating scheme to analyze NRP1 expression on Tregs (**A**) and frequency of NRP1-expressing Tregs (**B**) analyzed by flow cytometry. **B,** Each symbol represents the value obtained from individual HD or patient. Midlines represent the mean of the data. Orange symbol represents the value obtained from expanded TILs of patients with HNSCC. **C,** Effects of indicated agents (2 μmol/L) on the suppressive function of the indicated Tregs against autologous Tconvs, with the readout being Tconv proliferation by CTG assay. **D,** Inhibitory effects of indicated agents (2 μmol/L) on the suppressive function of intratumoral Tregs with different frequencies of NRP1$^+$ Tregs from patients with HNSCC against autologous Tconvs, with the readout being IL2 secretion from Tconvs. **C** and **D,** Results are depicted as the mean ± SEM of three independent experiments. Significance was tested using one-way ANOVA, followed by the Newman–Keuls *post hoc* test. **, $P < 0.01$; ***, $P < 0.001$ between the indicated groups; ns, not significant. IT, intratumoral.

on the surface with considerable variations of 2.68% to 15.7% from HNSCC and 1.69% to 18.6% from NSCLC (**Fig. 5B**). These data demonstrated the selective expression of NRP1 on intratumoral Tregs, but not on peripheral Tregs, in patients with HNSCC and NSCLC.

For *in vitro* functional analysis, we expanded TILs from patients to obtain a large enough pool of intratumoral Tregs. We confirmed that NRP1 expression on expanded Tregs was comparable with that on fresh Tregs in the two tumors (Supplementary Fig. S6), as observed for mouse Tregs (Supplementary Fig. S3A). Intriguingly, NRP1$^-$ Tregs purified from the PBMCs of healthy donors or patients with NSCLC showed no suppressive function against the proliferation of autologous CD4$^+$CD25$^-$ T cells, whereas NRP1$^+$ Tregs from tumors of patients with NSCLC suppressed CD4$^+$CD25$^-$ T-cell proliferation (**Fig. 5C**). Fc(AAG)-TPP11 decreased the suppressive function of intratumoral NRP1$^+$ Tregs from patients with NSCLC (**Fig. 5C**). We further assessed the suppressive function of the intratumoral Tregs pool with a different frequency of NRP1$^+$ Tregs, purified from TILs of patients with HNSCC by determining IL2 secretion from cocultured CD4$^+$CD25$^-$ Tconvs. Whereas the frequency of NRP1$^+$ Tregs was correlated with the suppressive activity, Fc(AAG)-TPP11 impeded the suppressive function in proportion to the frequency of intratumoral NRP1$^+$ Tregs (**Fig. 5D**). These results demonstrated that Fc(AAG)-TPP11 inhibited the function of intratumoral NRP1$^+$ Tregs in human cancers.

Discussion

As NRP1 plays a critical role in the stability and function of intratumoral Tregs, antagonizing NRP1 to inhibit NRP1$^+$ Tregs has been suggested as an effective approach for limiting Treg-mediated cancer progression (15, 17). In this study, we demonstrated that an effector-silent Fc(AAG)-fused NRP1-specific peptide, Fc(AAG)-TPP11, exerted antitumor activity by inhibiting intratumoral NRP1$^+$ Treg function rather than by systemically depleting NRP1$^+$ Tregs. NRP1-specific binding of Fc(AAG)-TPP11 on NRP1$^+$ Tregs triggered the cellular internalization of NRP1, downregulating its cell-surface

expression, and blocked the interactions of Treg-expressed NRP1 with its stabilizing ligand Sema4a, impairing the NRP1-dependent suppressive function of Tregs. Fc(AAG)-TPP11 efficiently inhibited tumor growth in immunocompetent mice bearing syngeneic CT26 and B16F10 tumors at a comparable potency to the anti–CTLA-4 9D9 Ab. The NRP1$^+$ Treg-restricted inhibitory activity of Fc(AAG)-TPP11 was validated by coadoptive transfer of both CD8$^+$ T cells and Tregs into T cell–deficient Balb/c nude mice with preestablished CT26 tumors. Treatment with Fc(AAG)-TPP11 attenuated NRP1-dependent Treg function and proliferation in the TME, but not in the tdLN and spleen, as exhibited by decreased expression of suppressive molecules such as IL10 and CD73 and the proliferation marker Ki-67 only for intratumoral Tregs. Fc(AAG)-TPP11 induced an unstable Treg phenotype in the TME, as detected by reduced Foxp3 expression and enhanced IFNγ production only for intratumoral Tregs. Subsequently, tumor-infiltrated CD8$^+$ and CD4$^+$Foxp3$^-$ T cells in Fc(AAG)-TPP11–treated TBM acquired a more functional phenotype characterized by upregulation of Ki-67, IFNγ, IL2, TNFα, and/or granzyme B. Consequently, Fc(AAG)-TPP11 increased the ratio of effector T cells to Tregs in the TME, explaining the antitumor activity of Fc(AAG)-TPP11.

Some clinical studies have suggested that the antitumor activity of anti–CTLA-4 ipilimumab therapy is mediated mainly by depleting intratumoral CTLA-4$^+$ Tregs through Fc-mediated effector functions and activation of effector T cells in the TME (9, 10, 43, 44), as observed in the preclinical murine models (7, 8). The anti–CTLA-4 Ab therapy does not deplete intratumoral Tregs in human cancers regardless of the Ab effector function (11), prompting further investigations on the precise mechanism underlying the clinical activity of anti–CTLA-4 immunotherapy (45). In this study, to exclude the potential mechanism of depleting NRP1$^+$ Tregs by Fc-mediated effector functions, an effector function–deficient Fc(AAG) variant was used to generate the NRP1-targeting agent, Fc(AAG)-TPP11. Compared with the anti-murine CTLA-4 9D9 mouse IgG2a Ab with full effector functions, used as a surrogate Ab of ipilimumab (7), Fc(AAG)-TPP11 showed nearly equivalent antitumor activity in CT26- and B16F10-TBM models, although the dosing regimens differed (**Fig. 2**). This suggests that inhibition of the function and stability of intratumoral NRP1$^+$ Tregs by NRP1 blockade is a promising therapeutic strategy, comparable to the Treg-depleting approach. Fc(AAG)-TPP11 elicited no significant loss in body weight or elevation of liver enzymes in both CT26- and B16F10-TBM. NRP1 expression was much higher in intratumoral Tregs than in peripheral Tregs. Thus, the lack of toxicity of Fc(AAG)-TPP11 was ascribed to the preferential targeting to NRP1^{high} Tregs in tumor site rather than NRP1^{low} Tregs in peripheral sites, as observed in both CT26- and B16F10-TBM (**Fig. 3B**). This was further supported by the tumor site–specific effect of Fc(AAG)-TPP11 on enhancement of the frequency and effector function of CD8$^+$ and CD4$^+$Foxp3$^-$ T cells, but not those in tdLN and spleen. Targeting of peripheral NRP1^{low} Tregs by Fc(AAG)-TPP11 will not evoke undesirable autoimmunity because NRP1 in Tregs is dispensable for the suppression of autoimmunity and maintenance of immune homeostasis (15, 17). Given that CTLA-4 is expressed on both peripheral and intratumoral Tregs in addition to activated effector T cells in human cancers (9), anti–CTLA-4 Ab therapy influences the activity of both Tregs and activated effector T cells (2, 11, 30). The dual activity of anti–CTLA-4 Ab might explain the irAEs observed in a subset of patients, although it is unclear whether the irAEs could be attributed to the depletion of Tregs or activation of effector T cells, or both (2, 45). NRP1 is overexpressed on intratumoral Tregs in human cancers, but barely expressed on peripheral Tregs (**Fig. 5B**). In this context, Fc(AAG)-TPP11 may be a safer agent that selectively restrains intratumoral NRP1$^+$ Tregs with no negative impacts on peripheral Tregs; however, this should be evaluated in human clinical settings.

It is important to determine whether the potent antitumor immunity of Fc(AAG)-TPP11 observed in mice is feasible in humans. Unlike in mouse Tregs (17, 21, 35), NRP1 was expressed to various extents only on the surface of intratumoral Tregs from patients with NSCLC and HNSCC, but not on peripheral blood Tregs from healthy donors and cancer patients (**Fig. 5B**). The suppressive function of intratumoral Tregs closely correlated with the frequency of NRP1$^+$ Tregs among TILs (**Fig. 5D**), consistent with previous observations that NRP1 expression in intratumoral Tregs was correlated with poor prognosis in both melanoma and HNSCC (15). These results suggest that NRP1 is a functional marker for intratumoral Tregs in human cancers. The inhibitory activity of Fc(AAG)-TPP11 was restricted to intratumoral NRP1$^+$ Tregs rather than NRP1$^-$ Tregs in PBMCs and proportional to the frequency of intratumoral NRP1$^+$ Tregs (**Fig. 5C** and **D**), suggesting that Fc(AAG)-TPP11 exerts antitumor activity by selectively inhibiting intratumoral NRP1$^+$ Tregs, while maintaining peripheral immune tolerance in humans.

In conclusion, we have demonstrated that the anti-NRP1 antagonistic Fc(AAG)-TPP11 exerts potent antitumor activity by inhibiting intratumoral NRP1$^+$ Treg function and stability in mouse tumor models. In human cancers, NRP1 expression was barely detected on peripheral Tregs but restricted to functional intratumoral Tregs, suggesting that NRP1 is an attractive molecular target for intratumoral Treg inhibition. Our results indicate that antagonizing NRP1 to inhibit intratumoral NRP1$^+$ Tregs is advantageous in terms of specificity and safety compared with other targets expressed in both peripheral and intratumoral Tregs, including CTLA-4.

Disclosure of Potential Conflicts of Interest

K. Jung, J.-A. Kim, Y.-J. Kim, and Y.-S. Kim are inventors on a patent application (PCT/KR2018/010487) related to the technology described in this work. No potential conflicts of interest were disclosed by the other authors.

Authors' Contributions

Conception and design: K. Jung, C.-H. Kim, Y.-S. Kim
Acquisition of data (provided animals, acquired and managed patients, provided facilities, etc.): K. Jung, J.-A. Kim, Y.-J. Kim, H.W. Lee, C.-H. Kim, S. Haam
Analysis and interpretation of data (e.g., statistical analysis, biostatistics, computational analysis): K. Jung, J.-A. Kim, Y.-J. Kim, H.W. Lee, Y.-S. Kim
Writing, review, and/or revision of the manuscript: K. Jung, J.-A. Kim, Y.-J. Kim, H.W. Lee, Y.-S. Kim
Administrative, technical, or material support (i.e., reporting or organizing data, constructing databases): H.W. Lee, C.-H. Kim, S. Haam
Study supervision: C.-H. Kim, Y.-S. Kim

Acknowledgments

This work was supported by National Research Foundation grants (2016R1A2A2A05005108 and 2014M3C1A3051470; to Y.-S. Kim), funded by the Ministry of Science, ICT and Future Planning, and the Korea Health Technology R&D Project (HI16C0992), funded by the Korea Health Industry Development Institute, Republic of Korea.

The costs of publication of this article were defrayed in part by the payment of page charges. This article must therefore be hereby marked *advertisement* in accordance with 18 U.S.C. Section 1734 solely to indicate this fact.

Received February 28, 2019; revised August 6, 2019; accepted September 19, 2019; published first September 25, 2019.

References

1. Sakaguchi S, Miyara M, Costantino CM, Hafler DA. FOXP3+ regulatory T cells in the human immune system. Nat Rev Immunol 2010;10:490–500.
2. Togashi Y, Shitara K, Nishikawa H. Regulatory T cells in cancer immunosuppression–implications for anticancer therapy. Nat Rev Clin Oncol 2019;16:356–71.
3. Liu C, Workman CJ, Vignali DA. Targeting regulatory T cells in tumors. FEBS J 2016;283:2731–48.
4. Takeuchi Y, Nishikawa H. Roles of regulatory T cells in cancer immunity. Int Immunol 2016;28:401–9.
5. Maherzi C, Onodi F, Tartour E, Terme M, Tanchot C. Strategies to reduce intratumoral regulatory T cells. In: Zitvogel L, Kroemer G, editors. Oncoimmunology: a practical guide for cancer immunotherapy. Cham (Switzerland): Springer; 2018. p. 483–506.
6. Sharabi A, Tsokos MG, Ding Y, Malek TR, Klatzmann D, Tsokos GC. Regulatory T cells in the treatment of disease. Nat Rev Drug Discov 2018;17:823–44.
7. Selby MJ, Engelhardt JJ, Quigley M, Henning KA, Chen T, Srinivasan M, et al. Anti-CTLA-4 antibodies of IgG2a isotype enhance antitumor activity through reduction of intratumoral regulatory T cells. Cancer Immunol Res 2013;1:32–42.
8. Simpson TR, Li F, Montalvo-Ortiz W, Sepulveda MA, Bergerhoff K, Arce F, et al. Fc-dependent depletion of tumor-infiltrating regulatory T cells co-defines the efficacy of anti-CTLA-4 therapy against melanoma. J Exp Med 2013;210:1695–710.
9. Arce Vargas F, Furness AJS, Litchfield K, Joshi K, Rosenthal R, Ghorani E, et al. Fc effector function contributes to the activity of human anti-CTLA-4 antibodies. Cancer Cell 2018;33:649–63e4.
10. Romano E, Kusio-Kobialka M, Foukas PG, Baumgaertner P, Meyer C, Ballabeni P, et al. Ipilimumab-dependent cell-mediated cytotoxicity of regulatory T cells ex vivo by nonclassical monocytes in melanoma patients. Proc Natl Acad Sci U S A 2015;112:6140–5.
11. Sharma A, Subudhi SK, Blando J, Scutti J, Vence L, Wargo J, et al. Anti-CTLA-4 immunotherapy does not deplete FOXP3(+) regulatory T cells (Tregs) in human cancers. Clin Cancer Res 2019;25:1233–8.
12. Attia P, Phan GQ, Maker AV, Robinson MR, Quezado MM, Yang JC, et al. Autoimmunity correlates with tumor regression in patients with metastatic melanoma treated with anti-cytotoxic T-lymphocyte antigen-4. J Clin Oncol 2005;23:6043–53.
13. Phan GQ, Yang JC, Sherry RM, Hwu P, Topalian SL, Schwartzentruber DJ, et al. Cancer regression and autoimmunity induced by cytotoxic T lymphocyte-associated antigen 4 blockade in patients with metastatic melanoma. Proc Natl Acad Sci U S A 2003;100:8372–7.
14. Wolchok JD, Chiarion-Sileni V, Gonzalez R, Rutkowski P, Grob JJ, Cowey CL, et al. Overall survival with combined nivolumab and ipilimumab in advanced melanoma. N Engl J Med 2017;377:1345–56.
15. Overacre-Delgoffe AE, Chikina M, Dadey RE, Yano H, Brunazzi EA, Shayan G, et al. Interferon-gamma drives treg fragility to promote anti-tumor immunity. Cell 2017;169:1130–41e11.
16. Chaudhary B, Elkord E.Novel expression of Neuropilin 1 on human tumor-infiltrating lymphocytes in colorectal cancer liver metastases. Expert Opin Ther Targets 2015;19:147–61.
17. Delgoffe GM, Woo SR, Turnis ME, Gravano DM, Guy C, Overacre AE, et al. Stability and function of regulatory T cells is maintained by a neuropilin-1-semaphorin-4a axis. Nature 2013;501:252–6.
18. Prud'homme GJ, Glinka Y. Neuropilins are multifunctional coreceptors involved in tumor initiation, growth, metastasis and immunity. Oncotarget 2012;3:921–39.
19. Roy S, Bag AK, Singh RK, Talmadge JE, Batra SK, Datta K. Multifaceted role of neuropilins in the immune system: potential targets for immunotherapy. Front Immunol 2017;8:1228.
20. Terme M, Pernot S, Marcheteau E, Sandoval F, Benhamouda N, Colussi O, et al. VEGFA-VEGFR pathway blockade inhibits tumor-induced regulatory T-cell proliferation in colorectal cancer. Cancer Res 2013;73:539–49.
21. Hansen W, Hutzler M, Abel S, Alter C, Stockmann C, Kliche S, et al. Neuropilin 1 deficiency on CD4+Foxp3+ regulatory T cells impairs mouse melanoma growth. J Exp Med 2012;209:2001–16.
22. Kim YJ, Jung K, Baek DS, Hong SS, Kim YS. Co-targeting of EGF receptor and neuropilin-1 overcomes cetuximab resistance in pancreatic ductal adenocarcinoma with integrin beta1-driven Src-Akt bypass signaling. Oncogene 2017;36:2543–52.
23. Shin SM, Choi DK, Jung K, Bae J, Kim JS, Park SW, et al. Antibody targeting intracellular oncogenic Ras mutants exerts anti-tumour effects after systemic administration. Nat Commun 2017;8:15090.
24. Baecher-Allan C, Brown JA, Freeman GJ, Hafler DA. CD4+CD25high regulatory cells in human peripheral blood. J Immunol 2001;167:1245–53.
25. Kim YJ, Bae J, Shin TH, Kang SH, Jeong M, Han Y, et al. Immunoglobulin Fc-fused, neuropilin-1-specific peptide shows efficient tumor tissue penetration and inhibits tumor growth via anti-angiogenesis. J Control Release 2015;216:56–68.
26. Appleton BA, Wu P, Maloney J, Yin J, Liang WC, Stawicki S, et al. Structural studies of neuropilin/antibody complexes provide insights into semaphorin and VEGF binding. EMBO J 2007;26:4902–12.
27. Lo M, Kim HS, Tong RK, Bainbridge TW, Vernes JM, Zhang Y, et al. Effector-attenuating substitutions that maintain antibody stability and reduce toxicity in mice. J Biol Chem 2017;292:3900–8.
28. Schlothauer T, Herter S, Koller CF, Grau-Richards S, Steinhart V, Spick C, et al. Novel human IgG1 and IgG4 Fc-engineered antibodies with completely abolished immune effector functions. Protein Eng Des Sel 2016;29:457–66.
29. Jung K, Ha JH, Kim JE, Kim JA, Kim YJ, Kim CH, et al. Heterodimeric Fc-fused IL12 shows potent antitumor activity by generating memory CD8(+) T cells. Oncoimmunology 2018;7:e1438800.
30. Peggs KS, Quezada SA, Chambers CA, Korman AJ, Allison JP. Blockade of CTLA-4 on both effector and regulatory T cell compartments contributes to the antitumor activity of anti-CTLA-4 antibodies. J Exp Med 2009;206:1717–25.
31. Postow MA, Sidlow R, Hellmann MD. Immune-related adverse events associated with immune checkpoint blockade. N Engl J Med 2018;378:158–68.
32. Lin YC, Chang LY, Huang CT, Peng HM, Dutta A, Chen TC, et al. Effector/memory but not naive regulatory T cells are responsible for the loss of concomitant tumor immunity. J Immunol 2009;182:6095–104.
33. Yadav M, Louvet C, Davini D, Gardner JM, Martinez-Llordella M, Bailey-Bucktrout S, et al. Neuropilin-1 distinguishes natural and inducible regulatory T cells among regulatory T cell subsets in vivo. J Exp Med 2012;209:1713–22, S1–19.
34. Wang S, Gao X, Shen G, Wang W, Li J, Zhao J, et al. Interleukin-10 deficiency impairs regulatory T cell-derived neuropilin-1 functions and promotes Th1 and Th17 immunity. Sci Rep 2016;6:24249.
35. Bruder D, Probst-Kepper M, Westendorf AM, Geffers R, Beissert S, Loser K, et al. Neuropilin-1: a surface marker of regulatory T cells. Eur J Immunol 2004;34:623–30.
36. Overacre-Delgoffe AE, Vignali DAA. Treg fragility: a prerequisite for effective antitumor immunity? Cancer Immunol Res 2018;6:882–7.
37. Munn DH, Sharma MD, Johnson TS. Treg destabilization and reprogramming: implications for cancer immunotherapy. Cancer Res 2018;78:5191–9.
38. Pedroza-Gonzalez A, Verhoef C, Ijzermans JN, Peppelenbosch MP, Kwekkeboom J, Verheij J, et al. Activated tumor-infiltrating CD4+ regulatory T cells restrain antitumor immunity in patients with primary or metastatic liver cancer. Hepatology 2013;57:183–94.
39. Bauer CA, Kim EY, Marangoni F, Carrizosa E, Claudio NM, Mempel TR. Dynamic Treg interactions with intratumoral APCs promote local CTL dysfunction. J Clin Invest 2014;124:2425–40.
40. Yu GT, Bu LL, Zhao YY, Mao L, Deng WW, Wu TF, et al. CTLA4 blockade reduces immature myeloid cells in head and neck squamous cell carcinoma. Oncoimmunology 2016;5:e1151594.
41. Leach DR, Krummel MF, Allison JP. Enhancement of antitumor immunity by CTLA-4 blockade. Science 1996;271:1734–6.
42. Sandin LC, Eriksson F, Ellmark P, Loskog AS, Totterman TH, Mangsbo SM. Local CTLA4 blockade effectively restrains experimental pancreatic adenocarcinoma growth in vivo. Oncoimmunology 2014;3:e27614.
43. Jie HB, Schuler PJ, Lee SC, Srivastava RM, Argiris A, Ferrone S, et al. CTLA-4(+) Regulatory T cells increased in cetuximab-treated head and neck cancer patients suppress NK cell cytotoxicity and correlate with poor prognosis. Cancer Res 2015;75:2200–10.
44. Ribas A, Kefford R, Marshall MA, Punt CJ, Haanen JB, Marmol M, et al. Phase III randomized clinical trial comparing tremelimumab with standard-of-care chemotherapy in patients with advanced melanoma. J Clin Oncol 2013;31:616–22.
45. Quezada SA, Peggs KS. Lost in translation: deciphering the mechanism of action of anti-human CTLA-4. Clin Cancer Res 2019;25:1130–2.